Thermal Stability and CO_2 Uptake of Dicationic Ionic Liquids Containing 2-Cyanopyrrolide Anions

Junwon Park, Louise M. Cañada, and Joan F. Brennecke*

McKetta Department of Chemical Engineering, The University of Texas at Austin, Austin, TX 78712

jfb@che.utexas.edu

Abstract

Aprotic-heterocyclic anion (AHA) ionic liquids (ILs) have the potential to be separation and reaction media for carbon capture and utilization (CCU) processes. While CO_2 capture may occur at moderate temperatures (e.g., between ambient and 50 ºC), thermochemical conversion of the CO_2 requires good thermal stability of the ILs, so that they can withstand reaction at elevated temperatures. ILs with non-coordinating anions such as bis(trifluoromethylsulfonyl)imide ($[Tf_2N]^-$) have shown improved thermal stability when the cation is modified to have 2+ charge; i.e., so called dicationic ILs. To our knowledge, no previous studies have paired dications with AHAs. A series of dicationic ILs composed of di(tetraalkylphosphonium) cations with tributyl chains and linkers ranging from propyl to undecyl, paired with 2-cyanopyrrolide anions, do show improved thermal stability compared to their monocationic AHA IL equivalents. Interestingly, the dicationic ILs all have similar CO_2 uptake per anion, although exhibiting CO_2 capacity intermediate between monocationic ILs with the 2-cyanopyrrolide anion and tetraalkylphosphonium cations with longer (trihexyltetradecyl) and shorter (triethyloctyl) chains. This is consistent with differences in the standard entropy of reaction between the anion and CO_2. Like their monocationic AHA counterparts, dicationic AHA ILs are sensitive to presence of oxygen, which results in the formation of phosphine oxides, as determined by long-term isothermal stress tests with air purging.

TOC Graphic

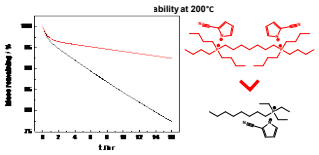

Introduction

Ionic Liquids (ILs) are salts that are liquid at temperatures below 373 K.[1] They are comprised of cations and anions which are usually bulky and asymmetric. This frustrates packing so they remain

liquid at relatively low temperatures. They generally have negligible vapor pressure and their high tunability (from the many choices of cations and anions) makes them suitable for various applications, including as media for gas separation and electrochemistry.[2,3] While ILs show potential for a wide variety of gas separations, there has been particularly strong interest in ILs as potential solvents for next generation carbon capture and utilization (CCU). Recent studies have shown ILs are competitive, in terms of capital and operating cost, for post-combustion carbon capture compared to advanced aqueous amines.[4] ILs do not contaminate the cleaned flue gas stream due to their negligible vapor pressure and energy consumption is less, primarily due to the weaker binding between the CO_2 and the solvent and not needing a co-solvent (water for aqueous amines), that consumes energy when it evaporates in the stripper.

Aprotic-heterocyclic anion (AHA) ILs, which react stoichiometrically with CO_2 at relatively low partial pressures (~1 bar) without dramatic viscosity increase, are promising solvents for CCU.[5] One can tune the enthalpy of reaction (ΔH_{rxn}) of the IL with CO_2 over a wide range by incorporating different electron withdrawing and donating substitutents.[6]

Additionally, recent studies have shown that captured CO_2 that is complexed with the capture solvent can be reduced to carbon monoxide, formate, methane and/or methanol within the liquid phase without separation of the CO_2 from the capture solvent, using catalysts at temperature higher than 150°C.[7–11] We anticipate that AHA ILs could also be used as a capture and reaction medium given the similarity in the CO_2 capture chemistry. In order to use AHA ILs for thermochemical reduction of CO_2, they need to have high thermal stability to withstand the reaction conditions for the thermocatalysis.

Unfortunately, AHA ILs have shown significant weight loss over relatively short periods of time at temperatures 100 K lower than literature reported decomposition temperatures. For

instance, trihexyltetradecylphosphonium 2-cyanopyrrolide ([P_{66614}][2CNPyr]) shows ~20% mass loss after 16 hours of isothermal stress at 468 K, which is 121 K lower than the reported decomposition temperature of 589 K.[12] A number of research groups have designed more thermally stable ILs.[13–16] For example, ILs with tetraarylphosphonium cations can have decomposition temperatures 25 K higher than their tetraalkylphosphonium equivalents (e.g., [PPh_4][Tf_2N] and [P_{66614}][Tf_2N]).[14,17] Thermal stability of ILs is affected by a number of factors, including selection of the ion pair and length of the chains on the cation.[18] For instance, phosphonium cations are more thermally stable than imidazolium cations when paired with halide anions ([P_{66614}][Br] > 1-butyl-3-methylimidazolium bromide, [BMIM][Br]). One promising design option is cation modification to have dicationic ILs. Dicationic ILs contain two cations tethered by a linker (e.g., an alkyl chain) to form a cation with a 2+ charge. When paired with bis(trifluoromethylsulfonyl)imide ($[Tf_2N]^-$) anions, dicationic ILs show 20 K to 65 K greater thermal stability than the equivalent monocationic ILs due to their greater charge and intermolecular interactions, and smaller free volume.[19–21] Dicationic ILs also exhibit wider electrochemical windows than equivalent monocationic ILs, making them a possible candidates for battery applications.[22] Though they have better stability, both thermally and electrochemically, dicationic ILs have several disadvantages, such as higher viscosities and melting point temperatures than equivalent monocationic ILs.[20] Previous studies have explored dicationic ILs, both experimentally and computationally, for their potential use in CO_2 capture.[23,24] However, to our knowledge there has not been a study of thermal stability and CO_2 uptake of dicationic ILs paired with AHAs. We anticipate that pairing dications with AHAs will also improve thermal stability compared to the monocationic equivalents. This study aims to understand the physicochemical properties of dicationic AHA ILs, including their long and short-term thermal stability, as well as their CO_2 capture capacity.

Materials and Methods

Materials

All the ILs were synthesized in house using the methods described in the Supporting Information. NMR spectra (^{1}H, ^{13}C, and ^{31}P) of the ILs and their respective precursors can be found in Figures S1-S42. All ILs synthesized for this study, with their estimated purity and bromide content measured with a Thermo Scientific Dionex ICS-5000^{+} ion chromatography system, are listed in Table 1. The dications were chosen to have tributyl groups with various length linkers for ease of synthesis. $[P_{2228}]^{+}$ and $[P_{66614}]^{+}$ monocations were chosen because there is wide availability of literature data for AHAs ILs with these cations. $[P_{4444}]^{+}$ was chosen because the chain length of the dication precursor (tributylphosphine) is C_4.

Triethylphosphine (99% purity) and tributylphosphine (99% purity) were purchased from STREM Chemicals; tributylphosphine (95% purity), 1-bromooctane (98% purity), 1,3-dibromopropane (98% purity), pyrrole-2-carbonitrile (99% purity), Amberlite IRN78 (nuclear grade), and toluene (99.5% purity) were purchased from Alfa Aesar; pyrrole-2-carbonitrile (98% purity) was purchased from Matrix Scientific; 1,5-dibromopentane (98% purity) was purchased from BeanTown Chemical; 1,7-dibromoheptane (98% purity), 1,9-dibromononane (97% purity), 1,11-dibromoundecane (96% purity) and tetrabutylphosphonium bromide (99% purity) were purchased from TCI America; trihexyl(tetradecyl)phosphonium bromide (95% purity) was purchased from IOLITEC; pyrrole-2-carbonitrile (99% purity) and Amberlite IRN78 (nuclear grade) were purchased from Thermo Scientific; acetonitrile (>99.9% purity) was purchased from Honeywell; and anhydrous methanol

(99.8% purity) was purchased from VWR. All chemicals and gases used for synthesis and experiments were used without further purification are listed on Table 2.

Table 1. Structures, abbreviations, and full names of the ILs[a]

Nomenclature	Structure	Purity (wt%)	Bromide content (ppm)[b,c]
Triethyl(octyl)phosphonium 2-cyano-pyrrolide [P_{2228}][2CNPyr]	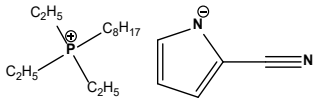	≥98%	408
Tetrabutylphosphonium 2-cyano-pyrrolide [P_{4444}][2CNPyr]	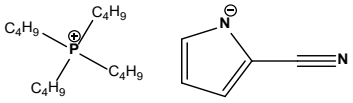	≥98%	421
Trihexyl(tetradecyl)phosphonium 2-cyano-pyrrolide [P_{66614}][2CNPyr]	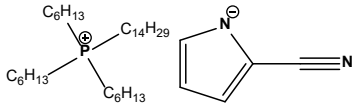	≥98%	2194
Propane-1,3-diylbis(tributylphosphonium) bis(2-cyano-pyrrolide) [$C_3(P_{444})_2$][$(2CNPyr)_2$]	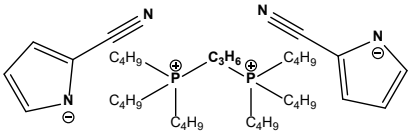	≥98%	143
Pentane-1,5-diylbis(tributylphosphonium) bis(2-cyano-pyrrolide) [$C_5(P_{444})_2$][$(2CNPyr)_2$]	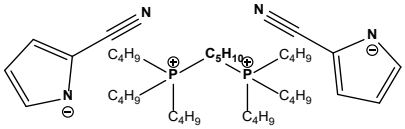	≥98%	287
Heptane-1,7-diylbis(tributylphosphonium) bis(2-cyano-pyrrolide) [$C_7(P_{444})_2$][$(2CNPyr)_2$]	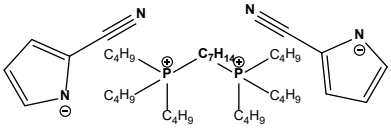	≥98%	583
Nonane-1,9-diylbis(tributylphosphonium) bis(2-cyano-pyrrolide) [$C_9(P_{444})_2$][$(2CNPyr)_2$]	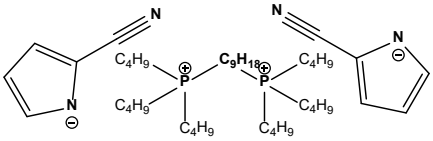	≥98%	359

Undecane-1,11-diylbis(tributylphosphonium) bis(2-cyano-pyrrolide) $[C_{11}(P_{444})_2][(2CNPyr)_2]$	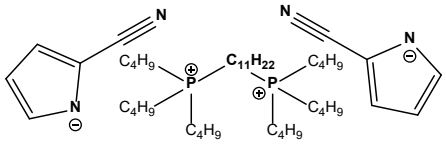	≥98%	465

[a]All ILs were synthesized in house
[b]Bromide contents reported are in mass fraction and determined using ion chromatography (IC)
[c]All ILs were subjected to vacuum (~3×10^{-3} mbar) for 48 hours prior to IC measurements

Table 2. Precursors and chemicals used for synthesis and experiments

Chemical	CAS no.	Source	Purity	Analysis method
Cation precursors				
Triethylphosphine	554-70-1	STREM Chemicals	99%	GC[a]
Tributylphosphine	998-40-3	STREM Chemicals	99%	GC[a]
		Alfa Aesar	95%	GC[a]
Tetrabutylphosphonium bromide	3115-68-2	TCI America	99%	Argentometric Titration
Trihexyl(tetradecyl)phosphonium bromide	654057-97-3	IOLITEC	95%	NMR[b]
1-bromooctane	111-83-1	Alfa Aesar	98%	GC[a]
1,3-dibromopropane	109-64-8	Alfa Aesar	98%	GC[a]
1,5-dibromopentane	111-24-0	BeanTown Chemical	98%	GC[a]
1,7-dibromoheptane	4549-31-9	TCI America	98%	GC[a]
1,9-dibromononane	4549-33-1	TCI America	97%	GC[a]
1,11-dibromoundecane	16696-65-4	TCI America	96%	GC[a]
Anion precursors				
Pyrrole-2-carbonitrile	4513-94-4	Alfa Aesar	99%	GC[a]
		Thermo Scientific	99%	GC[a]
		Matrix Scientific	98%	GC[a]
Chemicals used for synthesis				
Amberlite IRN78 (nuclear grade)	11128-95-3	Alfa Aesar		

Acetonitrile	75-05-8	Thermo Scientific Honeywell	>99.9%	GC[a]
Anhydrous methanol	67-56-1	VWR	99.8%	GC[a]
Gases used for experiments				
Carbon dioxide	124-38-9	Airgas	99.99%	
Nitrogen	7727-37-9	Airgas	99.999%	

[a]Gas Chromatography
[b]Nuclear Magnetic Resonance

Glass transition and melting point temperature

Glass transition temperatures (T_g) and melting point temperatures (T_{mp}) were measured with a Mettler-Toledo differential scanning calorimeter (DSC), model DSC 3. All ILs were dried at least 24 hours under vacuum (~3×10^{-3} mbar) prior to the measurement to vaporize any volatile substances within the IL. A small amount of IL (approximately 30 mg) was loaded into a 40 μL aluminum crucible. T_g is the midpoint of a small heat capacity change upon heating from an amorphous glass state to a liquid state, and T_{mp} is the starting point of the endothermic curve upon melting the crystalline solid. The aluminum crucible containing the IL was sealed with a pierced cover and dried in situ at 383.0 K for 45 minutes to evaporate any water sorbed during sample preparation. Then the sample was cooled to 153.0 K, where it was held for 3 minutes, followed by heating to 383.0 K at 10 K/min. The estimated uncertainty for both T_g and T_{mp} is 1.0 K.[6]

Density and viscosity

Density and viscosity were measured using an Anton Paar SVM 3001 Stabinger viscometer with the chemical upgrade kit. IL water content was measured with a Metrohm Karl Fischer coulometer

(917 KF) to confirm that the water content was below 1000 ppm prior to the measurement. Both density and viscosity were measured at 303.15 K, 313.15 K, 323.15 K, and 333.15 K. The SVM 3001 has an instrument uncertainty of 0.005 K, 0.00005 g/cm^3, and 0.1% for temperature, density, and viscosity, repectively.[25] Considering the purity of the ILs, we report the uncertainty of the density and the viscosity as 0.5% and 2%, respectively.

Volumetric CO_2 uptake

A custom-made pressure drop based volumetric apparatus was used to determine the CO_2 uptake capacity of the ILs. Approximately 1.5 g of IL was added to a reaction vessel with a magnetic stirrer (215.6 cm^3 excluding the volume displaced by the magnetic stirrer) under a nitrogen environment to minimize water and atmospheric CO_2 absorption. IL water content prior to loading was measured with a Metrohm Karl Fischer coulometer (917 KF) to confirm the water content was below 1000 ppm. The reaction vessel was connected to a reservoir with known volume (295.0 cm^3) and the IL was stirred continuously. The entire system was placed inside an oven (Yamato DKN602) and vacuum (~3×10^{-3} mbar) was pulled for 48 hours to further reduce water and any other volatile species in the system. Approximately 3000 mbar of CO_2 was introduced into the reservoir and oven temperature set to 333.2 K. The pressure and temperature of both reaction vessel and reservoir were determined using Heise model PM digital pressure indicators (5 mbar uncertainty), and type K thermocouples (Omega HH501DK, 0.5 K uncertainty), respectively. After the pressure and temperature equilibrated in the reservoir, CO_2 was introduced into the reaction vessel from the reservoir and allowed to equilibrate. The amount of CO_2 added to the reaction vessel from the

reservoir was calculated using the Lee-Kesler equation of state with known temperature, volume, and pressure.[26] The CO_2 uptake capacity of the IL was determined similarly in the reaction vessel after equilibrium was reached. More CO_2 was added repeatedly to the reaction vessel, ensuring equilibration after each addition, until the final pressure inside the reaction vessel was approximately 1 bar. The uncertainty of each CO_2 uptake measurement with this setup is 0.02 mol CO_2/mol anion, similar to our previous results.[27]

Short-term and long-term thermal stability

Both short-term and long-term thermal stability were measured using a Mettler-Toledo thermal gravimetric analyzer (TGA), model TGA/DSC 3+, under 100 mL/min nitrogen purging. All ILs were dried at least 24 hours under vacuum (~3×10^{-3} mbar) prior to the measurement. A small amount of IL (approximately 30 mg) was loaded into a 40 µL aluminum crucible. For short-term thermal stability, we report the onset temperature (T_{onset}), which is the temperature at the intersection of the initial weight baseline and a tangent to the weight versus temperature curve as fast decomposition occurs at a temperature ramp of 10 K/min. The main source of uncertainty in determining the T_{onset} is manually setting the tangent line, which results in 2.0 K uncertainty. For long-term thermal stability, we report weight percent loss after leaving the sample under thermal stress at the desired temperature for 16 hours. For both short-term and long-term thermal stress studies, the IL was dried in situ at 383 ± 1 K for 45 minutes prior to the experiment to evaporate as much of any remaining water and volatile species as possible. The main source of instrument uncertainty for long-term thermal stability measurements is from the TGA sample balance, which has a 0.01 wt% uncertainty. The long-term thermal stability of ILs in the presence of oxygen was

measured using 50 mL/min nitrogen + 50 mL/min air purging. The temperature profile was the same as used for the inert condition test.

Decomposition product analysis

An Agilent Technologies 6120 Single Quadrupole LC/MS coupled with electrospray (ESI) source and mass per charge ratio (m/z) range from 50 to 2000 was used to analyze the liquid residue following isothermal stress tests. The ESI-MS operated in positive and negative modes, with a gas temperature of 573 K, drying gas flowrate of 10.0 L/min, nebulizer pressure of 60 psig, and a capillary voltage of 3500 V. 1μL of sample mixture was injected.

Results and Discussion

First, we present the melting points and glass transition temperatures for all five of the new dicationic ILs, as well as $[P_{4444}][2CNPyr]$ for comparison. This is followed by the density, viscosity and CO_2 uptake at 333.2 K for the three dicationic ILs that are liquid (or metastable liquid) at room temperature. We then give the onset temperatures for decomposition for all ILs, followed by detailed long term thermal stability investigation of the three liquid dicationic ILs in both N_2 and air atmospheres.

Glass transition temperature, melting point, density, and viscosity

Thermophysical properties of the newly synthesized dicationic ILs show that the linker chain length affects the melting point of the ILs, but has negligible effect on T_g, density, and viscosity. Table 3 shows the T_g, T_{mp}, and their state at room temperature of the dicationic ILs in comparison to several monocationic ILs with the same anion. T_{mp} decreases as the linker chain length increases due to added conformational structures with longer linker chains.[15] For $[C_3(P_{444})_2][(2CNPyr)_2]$, the T_{mp} was determined by TGA instead of DSC as its T_{mp} was above the temperature range of DSC

experiments. The endotherm peak for T_{mp} *of* $[C_3(P_{444})_2][(2CNPyr)_2]$ from TGA can be found in Figure S43 in the Supporting Information. $[C_3(P_{444})_2][(2CNPyr)_2]$ and $[C_5(P_{444})_2][(2CNPyr)_2]$ had T_{mp} higher than room temperature, suggesting that the linker chain length should be carefully chosen to be longer than the alkyl chains on the trialkylphosphine precursor. In this case, C_3 and C_5 linker chains are shorter than or similar in length to the butyl chains on the starting trialkylphosphine precursor. Dicationic ILs with linker chain lengths greater than or equal to C_7 do not have melting points due to increased asymmetry with longer linker chain length. We conclude that C_7 is the critical linker chain length for synthesizing dicationic ILs with tributylphosphine. For monocationic ILs, $[P_{4444}]$[2CNPyr] has two endothermic peaks above room temperature, at 296 K and 328 K. To determine the origin of these observations, $[P_{4444}]$[2CNPyr] IL was annealed at 313 K for 20 minutes and then cooled to 153 K. The first endothermic peak at 296 K was not observed in this DSC experiment, indicating that the phase transition at 296 K is fusion of the metastable crystal. $[P_{4444}]$[2CNPyr] is solid at room temperature, undoubtedly due to the structural symmetry of the $[P_{4444}]^+$ cation. It was experimentally observed to remain in the solid phase at temperatures between the fusion of the metastable crystal (296 K) and T_{mp} (328 K), only becoming liquid once the temperature is over T_{mp}. $[P_{2228}]$[2CNPyr] and $[P_{66614}]$[2CNPyr] do not have melting points due to the asymmetry of the alkyl chains on the cations; they just have glass transition temperatures at 197 K and 193 K, respectively. These values compare reasonably well with previously published values of 196 K and 196 K, respectively.[28] Plots of DSC curves can be found in Figures S44-S51 of Supporting Information.

Table 3. Glass transition temperature (T_g) and melting point temperature (T_{mp}) of dicationic and corresponding monocationic ILs measured at atmospheric pressure and their state at room temperature.[a] N/A denotes a T_g or T_{mp} does not exist for this IL.

IL	T_g/K	T_{mp}/K	RT State
$[P_{2228}]$[2CNPyr]	197	N/A	Liquid

$[P_{4444}][2CNPyr]$	N/A	296/328[b]	Solid
$[P_{66614}][2CNPyr]$	193	N/A	Liquid
$[C_3(P_{444})_2][(2CNPyr)_2]$	N/A	452	Solid
$[C_5(P_{444})_2][(2CNPyr)_2]$	212	336	Solid
$[C_7(P_{444})_2][(2CNPyr)_2]$	225	N/A	Liquid
$[C_9(P_{444})_2][(2CNPyr)_2]$	224	N/A	Liquid
$[C_{11}(P_{444})_2][(2CNPyr)_2]$	210	N/A	Liquid

[a]The standard uncertainty is $u(T)$=1.0 K

[b]Two endothermic peaks are observed in the DSC measurements; see explanation in text

Densities and viscosities of the dicationic ILs, along with $[P_{2228}][2CNPyr]$ and $[P_{66614}][2CNPyr]$, are summarized in Table 4. Densities and viscosities of ILs that are solid at room temperature were not measured. The results are shown in comparison to values for monocationic ILs with the $[2CNPyr]^-$ anion in Figure 1. For monocationic ILs, the measured values agree with previously measurements within the experimental uncertainty.[5,28] Dicationic $[2CNPyr]^-$ ILs have ~2% and ~9% higher density than $[P_{2228}][2CNPyr]$ and $[P_{66614}][2CNPyr]$, respectively. Dicationic $[2CNPyr]^-$ ILs have viscosities ~6-26 times greater than the monocationc AHA ILs within the measured temperature range. Similar higher density and viscosity observations were made by Shirota et al.,[20] where they saw 4% higher density and 13-80 times greater viscosity with dicationic ILs paired with non-AHA anions. We attribute the higher viscosity to increased bulkiness of dications compared to monocations, as well as enhanced hydrogen-bonding interaction for dications.[20]

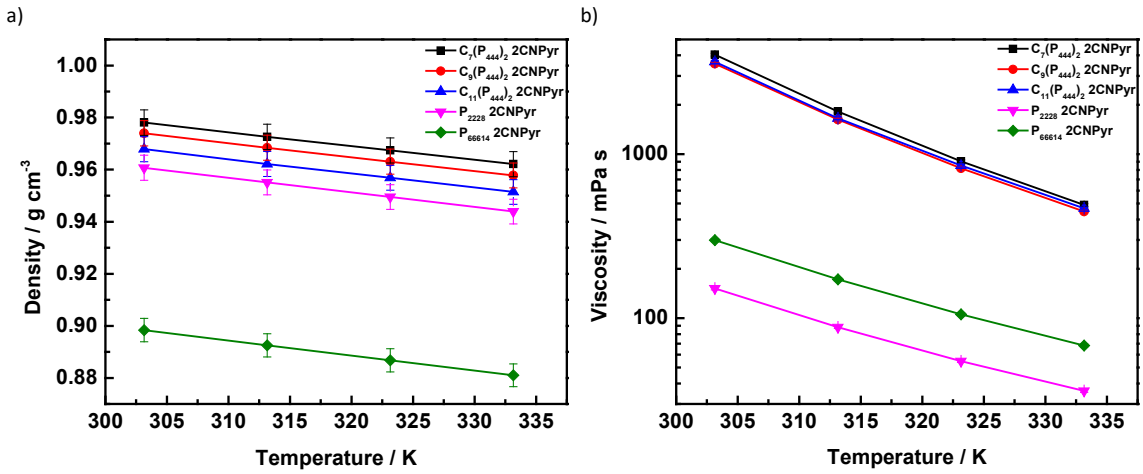

Figure 1. a) density and b) viscosity of dicationic AHA ILs in comparison to corresponding monocationic AHA ILs. Values for [P_{2228}][2CNPyr] and [P_{66614}][2CNPyr] are from Seo et al.[28] and Gurkan et al.,[5] respectively. Relative uncertainty for density and viscosity are 0.5% and 2%, respectively.

Table 4. Density and viscosity of dicationic [2CNPyr]$^-$ ILs measured at atmospheric pressure in comparison to equivalent monocationic ILs [a]

	[$C_7(P_{444})_2$] [(2CNPyr)$_2$] H_2O ppm = 221		**[$C_9(P_{444})_2$] [(2CNPyr)$_2$]** H_2O ppm = 64		**[$C_{11}(P_{444})_2$] [(2CNPyr)$_2$]** H_2O ppm = 119	
T/K	ρ/g·cm^{-3}	η/mPa·s	ρ/g·cm^{-3}	η/mPa·s	ρ/g·cm^{-3}	η/mPa·s
303.15	0.978	4040	0.974	3550	0.968	3650
313.15	0.973	1820	0.968	1620	0.962	1660
323.15	0.967	905	0.963	819	0.957	851
333.15	0.962	489	0.958	448	0.951	467
	[P_{2228}][2CNPyr] H_2O ppm = 244		**[P_{66614}][2CNPyr]** H_2O ppm = 182			
T/K	ρ/g·cm^{-3}	η/mPa·s	ρ/g·cm^{-3}	η/mPa·s		
303.15	0.961	152	0.898	299		
313.15	0.955	88.2	0.893	173		
323.15	0.950	54.8	0.887	106		
333.15	0.944	36.0	0.881	68.2		

[a] The standard uncertainties are $u(T)$=0.005 K, $u(\rho)$=0.005·ρ, and $u(\eta)$=0.02·η.

CO_2 uptake capacity at 333.2 K

All CO_2 uptake capacity measurements were done at an elevated temperature, 333.2 K, to increase the rate of mass transfer of CO_2 into the relatively viscous dicationic ILs. CO_2 uptake capacity (z)

for the three dicationic ILs on a mole CO_2 per mole anion basis is plotted in Figure 2 and exact values are reported in Table 5. Also shown in the figure are values for $[P_{2228}][2CNPyr]$ from Song et al.[27] and $[P_{66614}][2CNPyr]$ from Gurkan et al. (Supporting Information Table S2).[5] $[P_{2228}][2CNPyr]$ has the highest CO_2 uptake capacity at 333.2 K, reaching 0.71 mole CO_2 per mole anion at 1 bar CO_2 pressure. $[P_{66614}][2CNPyr]$ has the lowest uptake. All three dicationic $[2CNPyr]^-$ ILs had virtually identical CO_2 uptake capacities (i.e., the values fell within experimental uncertainties) that are between $[P_{2228}][2CNPyr]$ and $[P_{66614}][2CNPyr]$.

Each set of CO_2 uptake (z) data was fit with a Langmuir-type model as function of CO_2 pressure (P_{CO2}).

$$z = \frac{P_{CO_2}/H}{1-P_{CO_2}/H} + \frac{C_3 P_{CO_2} K_{eq}}{1+P_{CO_2} K_{eq}} \quad (1)$$

Where H (bar) is the Henry's law constant for physical dissolution of CO_2 in the IL, C_3 is the fraction of active IL, and K_{eq} is the equilibrium constant for complexation between CO_2 and an anion of the IL, as shown in Scheme 1. In this study (and for determination of C_3 and K_{eq},) the first term on the right-hand side of equation (1) was neglected since its contribution to the overall CO_2 uptake is generally less than the uncertainty of the CO_2 uptake values (0.02 mol CO_2/mol anion). For instance, an experimental estimate of the Henry's law constant for physically dissolved CO_2 in $[P_{66614}][2CNPyr]$ at 333.2 K is 100 bar.[5] At 1 bar CO_2 pressure this would contribute just 0.01 mol CO_2/mol IL. Equation (1) was then linearized giving equation (2).[29]

$$\frac{1}{z} = \frac{1}{C_3} + \frac{1}{P_{CO_2}} \frac{1}{C_3 K_{eq}} \quad (2)$$

C_3 and K_{eq} values can then be determined from plots of $\frac{1}{z}$ vs. $\frac{1}{P_{CO_2}}$, where the intercept is equal to $\frac{1}{C_3}$ and the slope is equal to $\frac{1}{C_3 K_{eq}}$. Plots of $\frac{1}{z}$ vs. $\frac{1}{P_{CO_2}}$ for all ILs can be found in Supporting Information Figure S52. C_3 and K_{eq} values used for Langmuir-type fitting are listed on Table 6.

The standard entropy of reaction (ΔS°_{rxn}) can be calculated assuming that the standard enthalpy of reaction (ΔH°_{rxn}) is a constant for any particular AHA anion and does not depend on the length of the alkyl chains on the cation, as we have done previously.[28] Using the general thermodynamic relationship $\Delta G^{\circ}_{rxn} = -RT\ln(K_{eq}) = \Delta H^{\circ}_{rxn} - T\Delta S^{\circ}_{rxn}$, where R is the gas constant, ΔS°_{rxn} can be calculated from experimental K_{eq} values and ΔH°_{rxn} (-45 kJ mol^{-1}, experimentally determined by Gurkan et al.[5]). These estimates for ΔS°_{rxn} are listed in Table. 6.

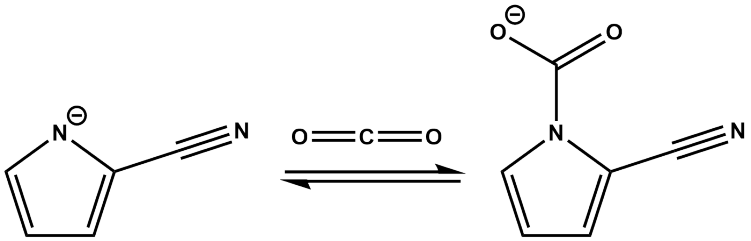

Scheme 1. CO_2 complexation with $[2CNPyr]^-$ anion

As mentioned above, the CO_2 capacities (mol CO_2/mol anion) of all three dicationic ILs are very similar and between the values for $[P_{2228}][2CNPyr]$ and $[P_{66614}][2CNPyr]$. Although dications are bulkier than $[P_{2228}]^+$ and $[P_{66614}]^+$, the shortest alkyl chains bonded to the phosphorous atoms (C_4 butyl chains) have lengths that lie between C_2 ($[P_{2228}]^+$) and C_6 ($[P_{66614}]^+$). The longer the majority chains on the cation, the lower the CO_2 capacity and the higher the absolute value of the standard entropy of reaction (ΔS°_{rxn}). The calculated ΔS°_{rxn} values for the three dicationic $[2CNPyr]^-$ ILs fall between $[P_{2228}][2CNPyr]$ and $[P_{66614}][2CNPyr]$. This suggests that increased reorganization of the alkyl chains on the cation is required for the anion to react with CO_2 when the alkyl chains are longer. Moreover, it appears that linkers of alkyl chains with seven or more carbon atoms are sufficiently long that the reorganization around the two anions of the dicationic ILs is essentially independent.

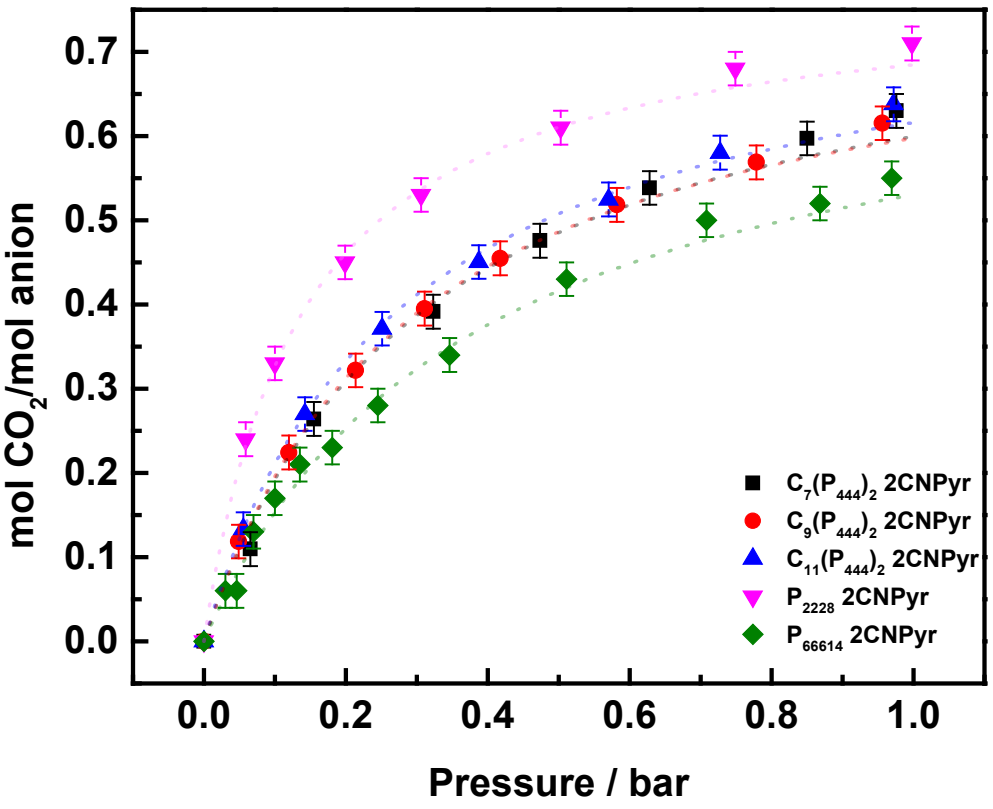

Figure 2. CO_2 uptake capacity at 333.2 K of dicationic $[2CNPyr]^-$ ILs. Uptake values for $[P_{2228}][2CNPyr]$ and $[P_{66614}][2CNPyr]$ are taken from Song et al.[27] and Gurkan et al.,[5] respectively. Uncertainty in CO_2 uptake capacity is 0.02 mol CO_2/mol anion.

Table 5. CO_2 uptake capacity of dicationic $[2CNPyr]^-$ ILs at 333.2 K.[a]

$[C_7(P_{444})_2][(2CNPyr)_2]$		**$[C_9(P_{444})_2][(2CNPyr)_2]$**		**$[C_{11}(P_{444})_2][(2CNPyr)_2]$**	
P/bar	mol CO_2/mol anion	*P*/bar	mol CO_2/mol anion	*P*/bar	mol CO_2/mol anion
0.000	0.00	0.000	0.00	0.000	0.00
0.065	0.11	0.049	0.12	0.056	0.13
0.155	0.26	0.120	0.22	0.142	0.27
0.323	0.39	0.214	0.32	0.251	0.37
0.474	0.48	0.311	0.40	0.387	0.45
0.628	0.54	0.418	0.45	0.570	0.52
0.850	0.60	0.582	0.52	0.727	0.58
0.976	0.63	0.779	0.57	0.972	0.64
		0.956	0.62		

[a]The standard uncertainties are *u(z)*=0.02 mol CO_2/mol anion, *u(P)*=0.005 bar, *u(T)*=0.5 K

Table. 6. K_{eq} (bar^{-1}) and C_3 (unitless) values fit to experimental CO_2 uptake data using eqn (1)

IL	K_{eq}/bar $^{-1}$	C_3	ΔS°_{rxn} /J·mol^{-1}·K^{-1}
$[C_7(P_{444})_2][(2CNPyr)_2]$	3.25	0.78	-125
$[C_9(P_{444})_2][(2CNPyr)_2]$	3.38	0.78	-125
$[C_{11}(P_{444})_2][(2CNPyr)_2]$	3.69	0.78	-124
$[P_{2228}][2CNPyr]$[a]	7.23	0.78	-119
$[P_{66614}][2CNPyr]$[a]	2.65	0.73	-127

[a] K_{eq} and C_3 values for $[P_{2228}][2CNPyr]$ and $[P_{66614}][2CNPyr]$ were determined using CO_2 uptake capacity values from Song et al.[27] and Gurkan et al.,[5] respectively.

Short-term and long-term thermal stability

Short-term thermal stability values for the five dicationic and three monocationic $[2CNPyr]^-$ ILs, as described by T_{onset} from TGA experiments, are tabulated in Table 7. The values for $[P_{2228}][2CNPyr]$ and $[P_{66614}][2CNPyr]$ agree reasonably well with previously published values of 567 K and 589 K, respectively.[28] $[P_{66614}][2CNPyr]$ had the highest T_{onset} (590 K) of the monocationic ILs; the ILs with shorter alkyl chains on the cation have T_{onset} values almost 20 K lower. With the exception of the one with the C_3 linker, all of the dicationic $[2CNPyr]^-$ ILs had significantly higher T_{onset} values than the monocationic $[2CNPyr]^-$ ILs. For instance, the T_{onset} for $[C_9(P_{444})_2][2CNpyr]$ is 36 K higher than $[P_{4444}][2CNpyr]$. Similar results have been noted in previous studies of dicationic ILs.[19,20] The higher thermal stability of dicationic ILs is widely believed to be due to greater charge and intermolecular interactions, higher density and viscosity, and smaller free volume.[20,21] Smaller free volume can give rise to a 'cage effect' which allows the recombination of fragments of decomposition.[20] Plots of short-term TGA curves can be found in Figures S53-S60 of Supporting Information.

Table 7. Onset temperature (T_{onset}) of monocationic and dicationic AHA ILs.[a]

IL	T_{onset}/K
$[P_{2228}][2CNpyr]$	572
$[P_{4444}][2CNpyr]$	571
$[P_{66614}][2CNpyr]$	590
$[C_3(P_{444})_2][2CNpyr]$	489
$[C_5(P_{444})_2][2CNpyr]$	596
$[C_7(P_{444})_2][2CNpyr]$	606
$[C_9(P_{444})_2][2CNpyr]$	607
$[C_{11}(P_{444})_2][2CNpyr]$	603

[a]The standard uncertainties are $u(T)$=2 K

Isothermal TGA was performed for $[P_{2228}][2CNPyr]$, $[P_{66614}][2CNPyr]$, $[C_7(P_{444})_2][(2CNPyr)_2]$, $[C_9(P_{444})_2][(2CNPyr)_2]$, and $[C_{11}(P_{444})_2][(2CNPyr)_2]$ at 413 K, 423 K, 433 K, 453 K and 473 K. The results at 473 K study are plotted in Figure 3. Isothermal TGA data for all of the ILs at different temperatures can be found in Figure S61-S65 of Supporting Information. The mass of the IL at the beginning of the 16-hour isothermal stress and the mass remaining after each hour of the experiment can be found in Tables S3-S7 of Supporting Information.

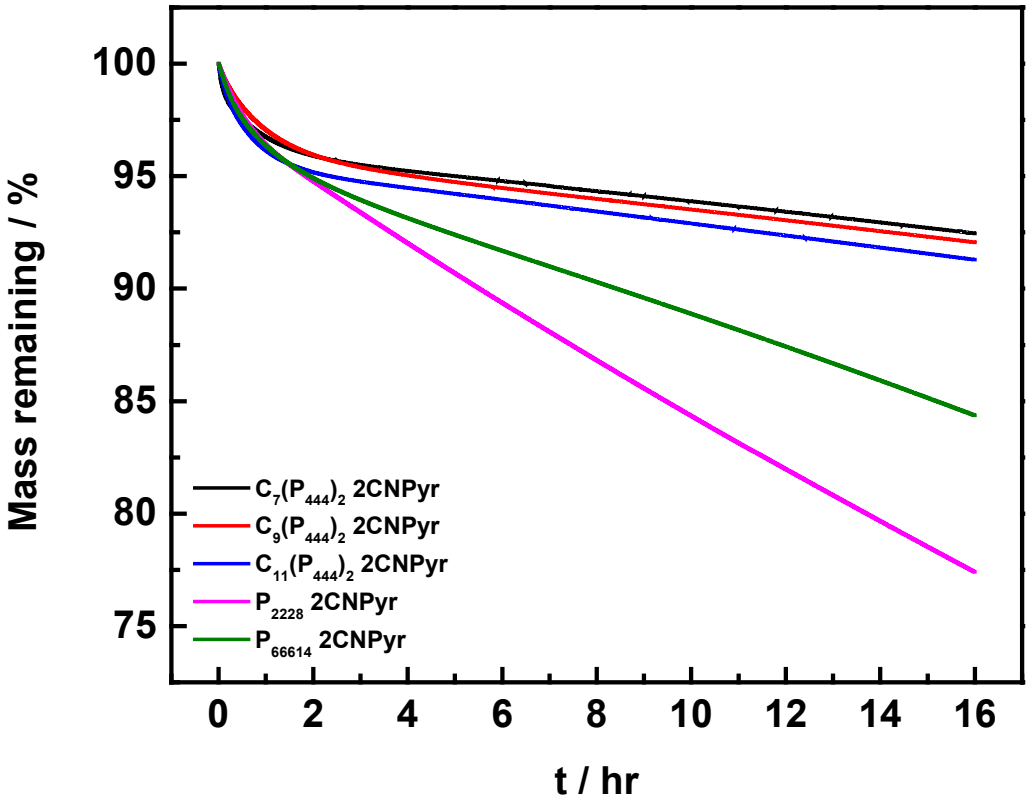

Figure 3. Isothermal TGA results for dicationic and monocationic $[2CNPyr]^-$ ILs at 473 K with a N_2 purge of 100 ml/min. The experimental uncertainty is 0.01 wt%.

$[P_{66614}][2CNPyr]$, the most thermally stable monocationic $[2CNPyr]^-$ IL based on T_{onset}, exhibited significantly less mass loss than $[P_{2228}][2CNPyr]$ after 16 hours of thermal stress, consistent with the trend in T_{onset} values. Long-term thermal stability of the dicationic $[2CNPyr]^-$ ILs is greatly improved over monocationic $[2CNPyr]^-$ ILs, with ~7 wt% more mass remaining after 16 hrs than $[P_{66614}][2CNPyr]$. The long-term thermal stabilities of all three dicationic $[2CNPyr]^-$ ILs are very similar, consistent with the T_{onset} data.

To quantify the long-term thermal stability, decomposition rates of the ILs are calculated using pseudo-zero-order kinetics, as has been done previously.[12,30–32] Pseudo-zero-order

decomposition assumes a linear weight loss of IL over time, which we do observe for all ILs studied after an initial rapid mass loss. Non-linear weight loss in the first several hours is attributed to degassing and vaporization of any gaseous or volatile substances that remain in the IL even after in-situ drying at 383 K. Another possible cause is fast decomposition resulting from very small amounts of hydroxide (OH^-) impurity in the IL since we proceed through an Amberlite anion hydroxide exchange in the synthesis of the ILs, before replacement with $[2CNPyr]^-$. OH^- is known to rapidly decompose phosphonium cations through a nucleophilic substitution mechanism at the phosphorus [S_N(P)] atom.[12,33–36] While impurities are always an issue in commercial processes, here we are interested in the intrinsic decomposition of the IL, rather than the influence of remaining volatiles or impurities that are specific to our particular synthesis procedure. As a result, we exclude the first 2 hours of data in the fitting of kinetic parameters for IL decomposition.

The pseudo-zero-order reaction kinetics expression is found in Equation (3).

$$\left(\frac{m_0 - m_t}{m_0}\right) \times 100 = kt \qquad \text{Equation (3)}$$

Where m_0 is mass of IL at the beginning of the thermal stress period (the 2 hr point for our analysis), and m_t is mass of IL at time t (for this study, the total time, t, is 16-2=14 hours), and k is rate constant. The rate constant's temperature dependence is described by the Arrhenius equation, Equation (4).

$$k = k_0 \exp\left(\frac{E_a}{RT}\right) \qquad \text{Equation (4)}$$

Where k_0 is frequency factor, E_a is activation energy, and R is gas constant. Therefore, a plot of $\ln(k)$ vs. $\frac{1}{T}$ allows one to calculate values for k_0 and E_a. Plots of $\ln(k)$ vs. $\frac{1}{T}$ for all of the ILs can be found in Figure S66 of Supporting Information. Table 8 shows the kinetic parameters for the decomposition of each IL. Although the uncertainty in the mass readings from the isothermal TGA

is just 0.01 wt%, the uncertainty in fitting the kinetic parameters is much larger due to the effects discussed above. Therefore, we only report these parameters to two significant figures.

Table 8. Decomposition rate kinetic parameters.[a]

IL	k/wt%·hr^{-1}					k_0/wt%·hr^{-1}	E_a/kJ·mol^{-1}
	413 K	423 K	433 K	453 K	473 K		
$[P_{2228}][2CNPyr]$	0.15	0.17	0.20	0.41	1.31	3.0×10^{6}	59
$[P_{66614}][2CNPyr]$	0.18	0.23	0.23	0.34	0.79	7.6×10^{3}	37
$[C_7(P_{444})_2][(2CNPyr)_2]$	0.17	0.16	0.20	0.16	0.30	4.8	12
$[C_9(P_{444})_2][(2CNPyr)_2]$	0.19	0.20	0.20	0.18	0.29	2.1	8.5
$[C_{11}(P_{444})_2][(2CNPyr)_2]$	0.17	0.17	0.17	0.19	0.41	7.7×10^{1}	22

[a]The standard uncertainties are $u(k)$=0.01 wt%·hr^{-1}, $u(k_0)$=0.05·k_0, $u(E_a)$=0.05·E_a

The decomposition rates of the three dicationic ILs and the two monocationic ILs are comparable at relatively low thermal stress (413 K, 423 K, and 433 K). However, as the thermal stress temperature increases, the decomposition rates of the monocationic AHA ILs are significantly greater than the dicationic AHA ILs. As a result, the k_0 values and activation energies for the monocationic AHA ILs are significantly larger than the dicationic AHA ILs.

To determine the effect of oxygen on long-term thermal stability of dicationic $[2CNPyr]^-$ ILs, an isothermal TGA experiment was conducted with 50 ml/min N_2 plus 50 ml/min air purge over $[C_{11}(P_{444})_2][(2CNPyr)_2]$. Figure 4 compares the mass loss with O_2 to a purely inert gas (N_2) environment. The mass remaining after each hour of the experiment can be found in Tables S8 of Supporting Information.

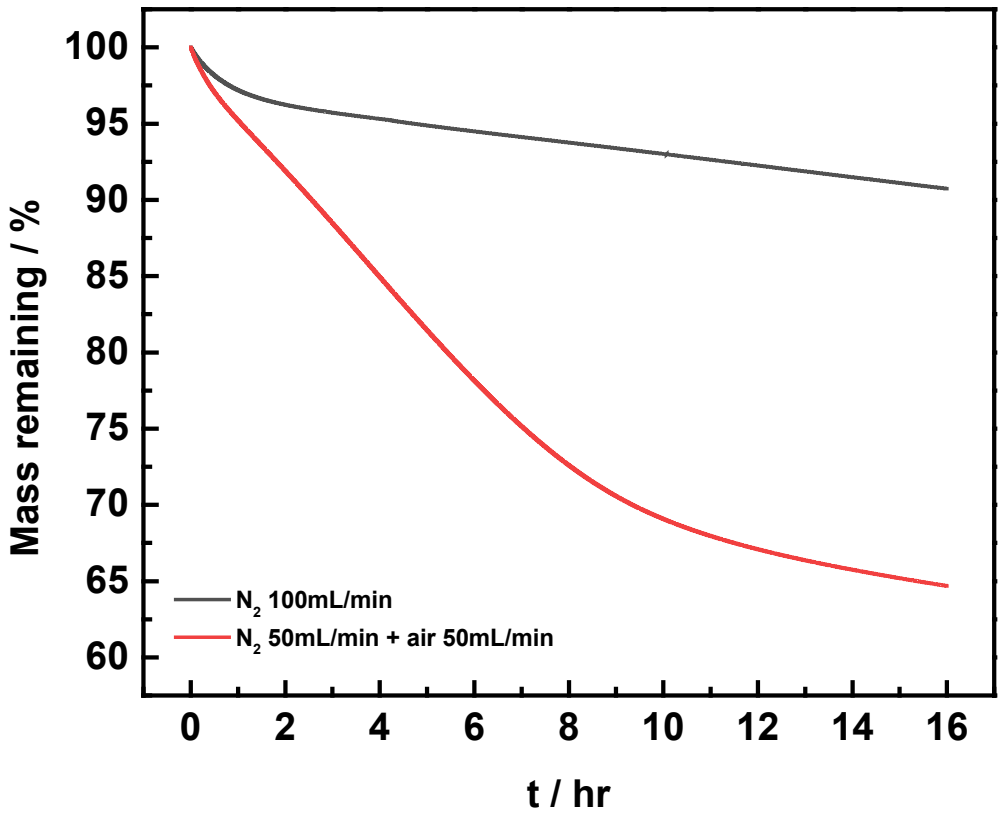

Figure 4. Isothermal TGA results for $[C_{11}(P_{444})_2][(2CNPyr)_2]$ at 473 K with a N_2 purge of 100 ml/min in comparison to air purge of 50 ml/min + N_2 purge of 50 ml/min. The experimental uncertainty is 0.01 wt%.

The presence of oxygen significantly decreases the long-term thermal stability of $[C_{11}(P_{444})_2][(2CNPyr)_2]$. With half of the purge gas being air, the IL lost 35 percent of its initial mass at 473 K in just 16 hours, which is about five times the mass loss in the presence of pure N_2. This is expected, based on previous studies of the thermal decomposition of tetra-alkylphosphonium salts in inert and oxidizing atmospheres.[12,33,36] In an inert atmosphere, nucleophilic substitution at the α-carbon or β-elimination (when a β-proton is abstracted by a basic anion) will result in the formation of trialkylphosphines.[12,33,36] It is well known that trialkylphosphines are air-sensitive, with many being pyrophoric, so great care must be taken when

synthesizing phosphonium ILs from trialkylphosphines. Thus, in the presence of O_2, one would expect any trialkylphosphines produced by nucleophilic substitution at the α-carbon or β-elimination to rapidly oxidize to trialkylphosphine oxide and a variety of other oxidation products. Note that trialkylphosphine oxide can also be produced in an inert atmosphere when OH^- attacks the phosphorus center.[12,33,36] Previously, we mentioned that small amounts of OH^- impurity from the IL synthesis could be contributing to the rapid, nonlinear mass loss for all the ILs under pure N_2 in the first several hours of the isothermal experiments. A final potential decomposition mechanism in an inert environment, possible only when a strongly basic anion is present, is α-proton abstraction to form phosphoranes.[37,38] Scheme 2 summarizes possible decomposition mechanisms of phosphonium dicationic and monocationic ILs with the $[2CNPyr]^-$ anion.

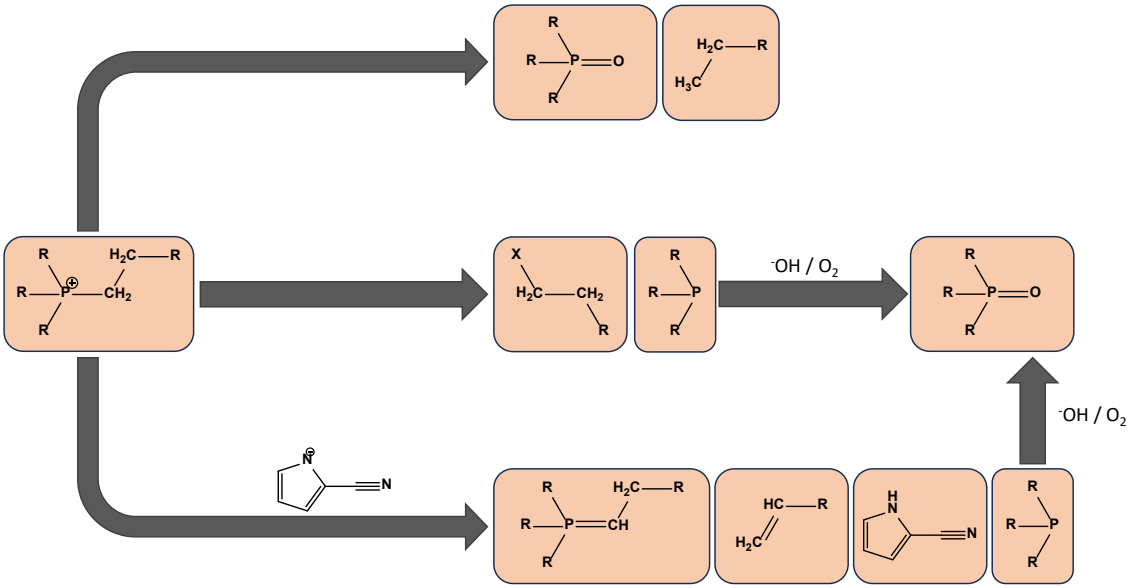

Scheme 2. Possible decomposition mechanisms of phosphonium dicationic and monocationic ILs with the $[2CNPyr]^-$ anion.

To confirm phosphine oxide formation, samples of $[C_{11}(P_{444})_2][(2CNPyr)_2]$ after pure N_2 or N_2 + air purging for 16 hours at 473 K were collected and analyzed by ESI-MS. Phosphine oxides are relatively nonvolatile (e.g., the trialkylphosphine oxides could only be detected with

GC when the injector has temperatures above 523 K[12]), so we would anticipate that some of the phosphine oxides formed would still be in the liquid phase. ESI-MS results are plotted in Figure 5.

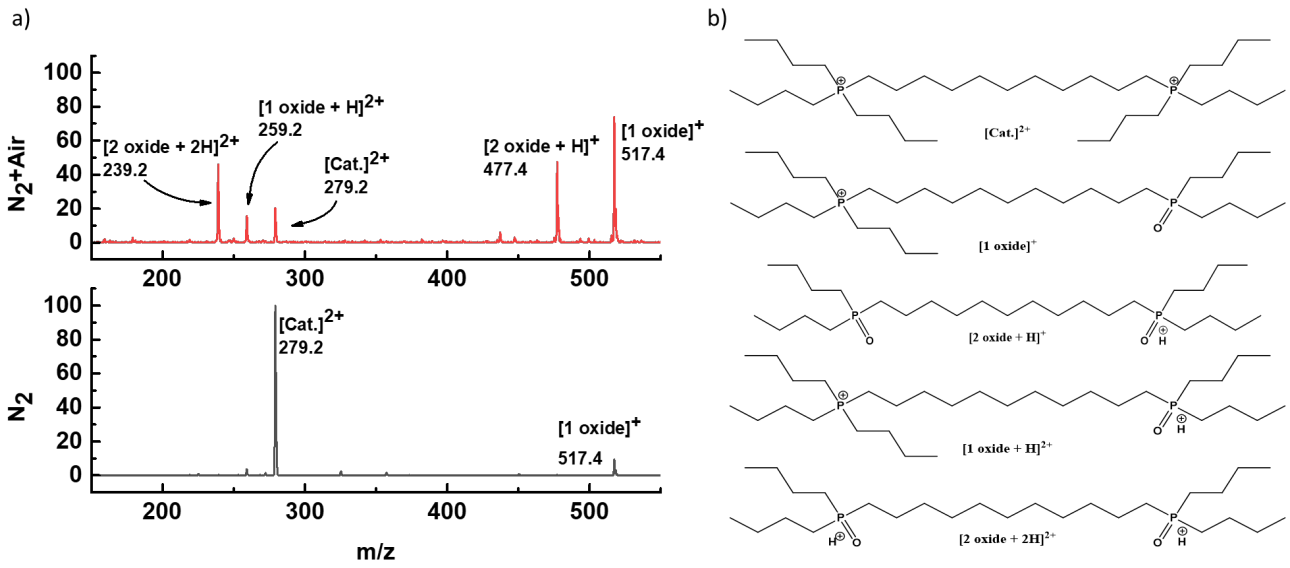

Figure 5. a) ESI-MS positive ion scan from 150 m/z to 550 m/z of $[C_{11}(P_{444})_2][(2CNPyr)_2]$ following isothermal TGA after 16 hours under different purging conditions at 473 K. N_2 + air purging (top red plot) has significantly higher formation of phosphine oxides than N_2 purging (bottom black plot). b) chemical structures corresponding to each peak identified in a), along with appropriate hydrogen adducts.

The liquid residue after heating at 473 K in an inert N_2 atmosphere is almost all the original $[C_{11}(P_{444})_2][(2CNPyr)_2]$. There is a very small peak corresponding to one of two phosphonium cations being oxidized to the phosphine oxide. This is consistent with a small amount of hydroxide impurity being present from the synthesis of the IL, or a trace amount of oxygen entering the TGA with the purge gas. By contrast, the liquid residue after heating in a mixture of N_2 and air contains a significant amount of a variety of phosphine oxide derivatives. This suggests that using phosphonium based AHA ILs in practice, whether they are monocationic or dicationic, will require strictly control and monitoring of oxygen to ensure the IL does not degrade in a short period of time under high temperature conditions.

Conclusion

Five different phosphonium based dicationic 2-cyanopyrrolide ILs were synthesized to compare their melting points, CO_2 uptake capacity, and thermal decomposition temperatures and rates with corresponding monocationic 2-cyanopyrrolide ILs. They all contained two tributylphosphonium cations joined by linkers of varying alkyl chain length. Three out of five dicationic 2-cyanopyrrolide ILs were liquid at room temperature. Except melting point temperature, the linker chain length did not significantly change the thermophysical properties of the various dicationic 2-cyanopyrrolide ILs. However, compared to monocationic 2-cyanopyrrolide ILs, dicationic 2-cyanopyrrolide ILs have significantly higher viscosities and slightly higher densities. The dicationic 2-cyanopyrrolide ILs had virtually identical CO_2 uptake capacities, regardless of linker length, that were significantly higher than monocationic 2-cyanopyrrolide ILs (i.e., triethyloctylphosphonium 2-cyanopyrrolide, $[P_{2228}][2CNPyr]$, and trihexyltetradecylphosphonium 2-cyanopyrrolide, $[P_{66614}][2CNPyr]$) per mole of IL because they contain two anions that can react with CO_2 per mole of IL. On the basis of moles of anion, the dicationic ILs had CO_2 uptake capacities intermediate between that of $[P_{66614}][2CNPyr]$ and $[P_{2228}][2CNPyr]$, consistent with increasing ΔS°_{rxn} with increasing length of the predominant chain on the cation. The dicationic 2-cyanopyrrolide ILs were more thermally stable than equivalent monocationic ILs. This was particularly pronounced for higher temperature isothermal decomposition tests, yielding activation energies for pseudo-zero-order decomposition twice as large for monocationic ILs than the dicationic ILs. As anticipated, the presence of oxygen resulted in a dramatic decrease in long-term thermal stability due to rapid formation of phosphine oxides. Overall, dicationic 2-cyanopyrrolide ILs show improvements in thermal stability relative to monocationic 2-cyanopyrrolide ILs, but at

the expense of a dramatic increase in viscosity. Increase in viscosity would lead to longer equilibration times for CO_2 uptake, which could be reduced by increasing gas-liquid surface area and increasing equilibration temperature. We conclude that phosphonium dicationic AHA ILs would be best suited for use in high temperature carbon capture and conversion applications where oxygen concentration is low. Other possible applications of dicationic AHA ILs are stationary phases for gas chromatography column and as heat transfer fluids.[19,39,40]

Acknowledgements

Support from the National Science Foundation under the ECO-CBET award 2133543 is acknowledged. The work was also partially funded by the Robert A. Welch Foundation (grant no. F-1945).

Associated Content

Supporting Information available. IL synthesis procedures, ^{1}H NMR, ^{13}C NMR, and ^{31}P NMR spectra for all newly synthesized ILs, density, viscosity, CO_2 uptake capacity, determination of Langmuir CO_2 uptake capacity parameters, isothermal TGA plots and data, and plots to determine pseudo-zero-order decomposition kinetics parameters.

References

(1) Lei, Z. Introduction: Ionic Liquids. *Chem. Rev.* **2017**, *117* (10), 6633–6635. https://doi.org/10.1021/acs.chemrev.7b00246.

(2) Bara, J. E.; Carlisle, T. K.; Gabriel, C. J.; Camper, D.; Finotello, A.; Gin, D. L.; Noble, R. D. Guide to CO2 Separations in Imidazolium-Based Room-Temperature Ionic Liquids. *Ind. Eng. Chem. Res.* **2009**, *48* (6), 2739–2751. https://doi.org/10.1021/ie8016237.

(3) Singh, S. K.; Savoy, A. W. Ionic Liquids Synthesis and Applications: An Overview. *J. Mol. Liq.* **2020**, *297*, 112038. https://doi.org/10.1016/j.molliq.2019.112038.

(4) Seo, K.; Tsay, C.; Hong, B.; Edgar, T. F.; Stadtherr, M. A.; Baldea, M. Rate-Based Process Optimization and Sensitivity Analysis for Ionic-Liquid-Based Post-Combustion Carbon Capture. *ACS Sustain. Chem. Eng.* **2020**, *8* (27), 10242–10258. https://doi.org/10.1021/acssuschemeng.0c03061.

(5) Gurkan, B.; Goodrich, B. F.; Mindrup, E. M.; Ficke, L. E.; Massel, M.; Seo, S.; Senftle, T. P.; Wu, H.; Glaser, M. F.; Shah, J. K.; Maginn, E. J.; Brennecke, J. F.; Schneider, W. F. Molecular Design of High Capacity, Low Viscosity, Chemically Tunable Ionic Liquids for CO_2 Capture. *J. Phys. Chem. Lett.* **2010**, *1* (24), 3494–3499. https://doi.org/10.1021/jz101533k.

(6) Keller, A. N.; Bentley, C. L.; Morales-Collazo, O.; Brennecke, J. F. Design and Characterization of Aprotic *N* -Heterocyclic Anion Ionic Liquids for Carbon Capture. *J. Chem. Eng. Data* **2022**, *67* (2), 375–384. https://doi.org/10.1021/acs.jced.1c00827.

(7) Kothandaraman, J.; Lopez, J. S.; Jiang, Y.; Walter, E. D.; Burton, S. D.; Dagle, R. A.; Heldebrant, D. J. Integrated Capture and Conversion of CO2 to Methanol in a Post-Combustion Capture Solvent: Heterogeneous Catalysts for Selective C□N Bond Cleavage. *Adv. Energy Mater. n/a* (n/a), 2202369. https://doi.org/10.1002/aenm.202202369.

(8) Kothandaraman, J.; Saavedra Lopez, J.; Jiang, Y.; Walter, E. D.; Burton, S. D.; Dagle, R. A.; Heldebrant, D. J. Integrated Capture and Conversion of CO_2 to Methane Using a Water-lean, Post-Combustion CO_2 Capture Solvent. *ChemSusChem* **2021**, *14* (21), 4812–4819. https://doi.org/10.1002/cssc.202101590.

(9) Kothandaraman, J.; A. Dagle, R.; Labarbier Dagle, V.; D. Davidson, S.; D. Walter, E.; D. Burton, S.; W. Hoyt, D.; J. Heldebrant, D. Condensed-Phase Low Temperature Heterogeneous Hydrogenation of CO 2 to Methanol. *Catal. Sci. Technol.* **2018**, *8* (19), 5098–5103. https://doi.org/10.1039/C8CY00997J.

(10) Kothandaraman, J.; Heldebrant, D. J. Towards Environmentally Benign Capture and Conversion: Heterogeneous Metal Catalyzed CO2 Hydrogenation in CO2 Capture Solvents. *Green Chem.* **2020**, *22* (3), 828–834. https://doi.org/10.1039/C9GC03449H.

(11) Maina, J. W.; Pringle, J. M.; Razal, J. M.; Nunes, S.; Vega, L.; Gallucci, F.; Dumée, L. F. Strategies for Integrated Capture and Conversion of CO2 from Dilute Flue Gases and the Atmosphere. *ChemSusChem* **2021**, *14* (8), 1805–1820. https://doi.org/10.1002/cssc.202100010.

(12) Huang, Y.; Chen, Z.; Crosthwaite, J. M.; N.V.K. Aki, S.; Brennecke, J. F. Thermal Stability of Ionic Liquids in Nitrogen and Air Environments. *J. Chem. Thermodyn.* **2021**, *161*, 106560. https://doi.org/10.1016/j.jct.2021.106560.

(13) Cassity, C. G.; Mirjafari, A.; Mobarrez, N.; Strickland, K. J.; O'Brien, R. A.; Davis, J. H. Ionic Liquids of Superior Thermal Stability. *Chem. Commun.* **2013**, *49* (69), 7590. https://doi.org/10.1039/c3cc44118k.

(14) Cassity, C. A.; Siu, B.; Soltani, M.; McGeehee, J. L.; Strickland, K. J.; Vo, M.; Salter, E. A.; Stenson, A. C.; Wierzbicki, A.; West, K. N.; Rabideau, B. D.; Davis, J. H. The Effect of Structural Modifications on the Thermal Stability, Melting Points and Ion Interactions for a Series of Tetraaryl-Phosphonium-Based Mesothermal Ionic Liquids. *Phys. Chem. Chem. Phys.* **2017**, *19* (47), 31560–31571. https://doi.org/10.1039/C7CP06278H.

(15) Patil, R. A.; Talebi, M.; Xu, C.; Bhawal, S. S.; Armstrong, D. W. Synthesis of Thermally Stable Geminal Dicationic Ionic Liquids and Related Ionic Compounds: An Examination of Physicochemical Properties by Structural Modification. *Chem. Mater.* **2016**, *28* (12), 4315–4323. https://doi.org/10.1021/acs.chemmater.6b01247.

(16) Talebi, M.; Patil, R. A.; Armstrong, D. W. Physicochemical Properties of Branched-Chain Dicationic Ionic Liquids. *J. Mol. Liq.* **2018**, *256*, 247–255. https://doi.org/10.1016/j.molliq.2018.02.016.

(17) Fillion, J. J.; Xia, H.; Desilva, M. A.; Quiroz-Guzman, M.; Brennecke, J. F. Phase Transitions, Decomposition Temperatures, Viscosities, and Densities of Phosphonium, Ammonium, and Imidazolium Ionic Liquids with Aprotic Heterocyclic Anions. *J. Chem. Eng. Data* **2016**, *61* (8), 2897–2914. https://doi.org/10.1021/acs.jced.6b00269.

(18) Cao, Y.; Mu, T. Comprehensive Investigation on the Thermal Stability of 66 Ionic Liquids by Thermogravimetric Analysis. *Ind. Eng. Chem. Res.* **2014**, *53* (20), 8651–8664. https://doi.org/10.1021/ie5009597.

(19) Breitbach, Z. S.; Armstrong, D. W. Characterization of Phosphonium Ionic Liquids through a Linear Solvation Energy Relationship and Their Use as GLC Stationary Phases. *Anal. Bioanal. Chem.* **2008**, *390* (6), 1605–1617. https://doi.org/10.1007/s00216-008-1877-3.

(20) Shirota, H.; Mandai, T.; Fukazawa, H.; Kato, T. Comparison between Dicationic and Monocationic Ionic Liquids: Liquid Density, Thermal Properties, Surface Tension, and Shear Viscosity. *J. Chem. Eng. Data* **2011**, *56* (5), 2453–2459. https://doi.org/10.1021/je2000183.

(21) Maton, C.; De Vos, N.; Stevens, C. V. Ionic Liquid Thermal Stabilities: Decomposition Mechanisms and Analysis Tools. *Chem. Soc. Rev.* **2013**, *42* (13), 5963–5977. https://doi.org/10.1039/c3cs60071h.

(22) Nirmale, T. C.; Khupse, N. D.; Kalubarme, R. S.; Kulkarni, M. V.; Varma, A. J.; Kale, B. B. Imidazolium-Based Dicationic Ionic Liquid Electrolyte: Strategy toward Safer Lithium-Ion Batteries. *ACS Sustain. Chem. Eng.* **2022**, *10* (26), 8297–8304. https://doi.org/10.1021/acssuschemeng.2c00767.

(23) Ma, J.; Zhou, Z.; Zhang, F.; Fang, C.; Wu, Y.; Zhang, Z.; Li, A. Ditetraalkylammonium Amino Acid Ionic Liquids as CO2 Absorbents of High Capacity. *Environ. Sci. Technol.* **2011**, *45* (24), 10627–10633. https://doi.org/10.1021/es201808e.

(24) Li, S.; Zhao, W.; Feng, G.; Cummings, P. T. A Computational Study of Dicationic Ionic Liquids/CO_2 Interfaces. *Langmuir* **2015**, *31* (8), 2447–2454. https://doi.org/10.1021/la5048563.

(25) Sariyerli, G. S.; Sakarya, O.; Akcadag, U. Y. Comparison Tests for the Determination of the Viscosity Values of Reference Liquids by Capillary Viscometers and Stabinger Viscometer SVM 3001. *Int. J. Metrol. Qual. Eng.* **2018**, *9*, 7. https://doi.org/10.1051/ijmqe/2018004.

(26) Lee, B. I.; Kesler, M. G. A generalized thermodynamic correlation based on three-parameter corresponding states. *AIChE J.* **1975**, *21* (3), 510–527. https://doi.org/10.1002/aic.690210313.

(27) Song, T.; Avelar Bonilla, G. M.; Morales-Collazo, O.; Lubben, M. J.; Brennecke, J. F. Recyclability of Encapsulated Ionic Liquids for Post-Combustion CO_2 Capture. *Ind. Eng. Chem. Res.* **2019**, *58* (12), 4997–5007. https://doi.org/10.1021/acs.iecr.9b00251.

(28) Seo, S.; DeSilva, M. A.; Xia, H.; Brennecke, J. F. Effect of Cation on Physical Properties and CO_2 Solubility for Phosphonium-Based Ionic Liquids with 2-Cyanopyrrolide Anions. *J. Phys. Chem. B* **2015**, *119* (35), 11807–11814. https://doi.org/10.1021/acs.jpcb.5b05733.

(29) Foo, K. Y.; Hameed, B. H. Insights into the Modeling of Adsorption Isotherm Systems. *Chem. Eng. J.* **2010**, *156* (1), 2–10. https://doi.org/10.1016/j.cej.2009.09.013.

(30) Salgado, J.; Villanueva, M.; Parajó, J. J.; Fernández, J. Long-Term Thermal Stability of Five Imidazolium Ionic Liquids. *J. Chem. Thermodyn.* **2013**, *65*, 184–190. https://doi.org/10.1016/j.jct.2013.05.049.

(31) Hao, Y.; Peng, J.; Hu, S.; Li, J.; Zhai, M. Thermal Decomposition of Allyl-Imidazolium-Based Ionic Liquid Studied by TGA–MS Analysis and DFT Calculations. *Thermochim. Acta* **2010**, *501* (1–2), 78–83. https://doi.org/10.1016/j.tca.2010.01.013.

(32) Kamavaram, V.; Reddy, R. G. Thermal Stabilities of Di-Alkylimidazolium Chloride Ionic Liquids. *Int. J. Therm. Sci.* **2008**, *47* (6), 773–777. https://doi.org/10.1016/j.ijthermalsci.2007.06.012.

(33) Deferm, C.; Bossche, A. V. den; Luyten, J.; Oosterhof, H.; Fransaer, J.; Binnemans, K. Thermal Stability of Trihexyl(Tetradecyl)Phosphonium Chloride. *Phys. Chem. Chem. Phys.* **2018**, *20* (4), 2444–2456. https://doi.org/10.1039/C7CP08556G.

(34) Bradaric, C. J.; Downard, A.; Kennedy, C.; Robertson, A. J.; Zhou, Y. Industrial Preparation of Phosphonium Ionic Liquids. *Green Chem.* **2003**, *5* (2), 143–152. https://doi.org/10.1039/B209734F.

(35) Fraser, K. J.; MacFarlane, D. R. Phosphonium-Based Ionic Liquids: An Overview. *Aust. J. Chem.* **2009**, *62* (4), 309–321. https://doi.org/10.1071/CH08558.

(36) Xie, W.; Xie, R.; Pan, W.-P.; Hunter, D.; Koene, B.; Tan, L.-S.; Vaia, R. Thermal Stability of Quaternary Phosphonium Modified Montmorillonites. *Chem. Mater.* **2002**, *14* (11), 4837–4845. https://doi.org/10.1021/cm020705v.

(37) Gohndrone, T. R.; Song, T.; DeSilva, M. A.; Brennecke, J. F. Quantification of Ylide Formation in Phosphonium-Based Ionic Liquids Reacted with CO_2. *J. Phys. Chem. B* **2021**, *125* (24), 6649–6657. https://doi.org/10.1021/acs.jpcb.1c03546.

(38) Oh, S.; Morales-Collazo, O.; Keller, A. N.; Brennecke, J. F. Cation–Anion and Anion–CO_2 Interactions in Triethyl(Octyl)Phosphonium Ionic Liquids with Aprotic Heterocyclic Anions (AHAs). *J. Phys. Chem. B* **2020**, *124* (40), 8877–8887. https://doi.org/10.1021/acs.jpcb.0c06374.

(39) Rabideau, B. D.; West, K. N.; Davis, J. H. Making Good on a Promise: Ionic Liquids with Genuinely High Degrees of Thermal Stability. *Chem. Commun.* **2018**, *54* (40), 5019–5031. https://doi.org/10.1039/c8cc01716f.

(40) Huang, K.; Han, X.; Zhang, X.; Armstrong, D. W. PEG-Linked Geminal Dicationic Ionic Liquids as Selective, High-Stability Gas Chromatographic Stationary Phases. *Anal. Bioanal. Chem.* **2007**, *389* (7), 2265–2275. https://doi.org/10.1007/s00216-007-1625-0.